Received: 13 May 2020 | Revised: 10 November 2020 | Accepted: 31 December 2020

DOI: 10.1002/stc.2701

WILEY

RESEARCH ARTICLE

Development of a low-power wireless acoustic emission sensor node for aerospace applications

Stephen Grigg[1] | **Rhys Pullin**[1] | **Matthew Pearson**[1] | **David Jenman**[2] | **Robert Cooper**[2] | **Andrew Parkins**[3] | **Carol Ann Featherston**[1]

[1]Cardiff School of Engineering, Cardiff University, Cardiff, UK

[2]BAE Systems, Rochester, UK

[3]HW Communications, Lancaster, UK

Correspondence
Stephen Grigg, School of Engineering, Cardiff University, Cardiff, CF24 3AA, UK.
Email: griggs@cardiff.ac.uk

Summary

Acoustic emission (AE) is the spontaneous release of energy caused by the growth of damage, the monitoring of which gives an indication of the presence of damage within a structure. The current standard for AE localisation is difficult to apply in a low-power system as sensors must either be wired together or Node's time synchronised, which is power intensive. This paper proposes the use of a method of bonding three piezoelectric sensors in a small triangular array, which has previously been shown by Aljets et al. to be capable of locating sources in simple structures. In this prior work the wave's A_0 mode was used to predict the angle of arrival and the distance the wave has travelled through single sensor modal analysis. This paper presents the development of hardware to apply this technique and testing that showed artificial sources could be located in simple plates to a good level of accuracy. The addition of complexity to structures significantly reduced accuracy. This prompted hardware modifications to use the S_0 mode for angle prediction. Testing showed that this significantly improved performance in a complex composite structure. The power consumption of the device is very low, consuming 0.33 mW in sleep mode, 17.44 mW whilst waiting for an event and 38 mW to record, process and transmit an event. This level of consumption has the potential to be self-powered via energy harvesting.

KEYWORDS

acoustic emission, aircraft, sensor node, structural health monitoring, wireless

1 | INTRODUCTION

Structural health monitoring (SHM) is the process of collecting data from a structure throughout its entire life, with the aim of identifying and tracking the growth of damage. Within the aircraft industry, this not only benefits safety but can also enable aircraft life extension and reduced maintenance downtime, both of which increase profitability.[1] Additionally, it has the potential to allow for optimally designed structures if confidence in the identification of damage can be ensured, reducing weight and therefore fuel consumption. A range of SHM techniques have been employed on aircraft

including strain, vibration and temperature monitoring.[2] These methods can be useful to assist with understanding the stresses put on the aircraft during its life, enabling predictions of damage locations.[1] They do not however inform of the presence of damage, something that ultrasonic techniques do.

One promising area of SHM which has previously been applied to aircraft structures is the monitoring of acoustic emission (AE).[1] AE is the spontaneous release of energy caused by the growth of damage. When an AE event occurs, it propagates as an ultrasonic wave through the structure.[3] These waves propagate through the aircraft and can be detected using piezoelectric sensors. Monitoring a structure for AE gives an indication of the presence of damage growth. AE monitoring is very common in bridges[4] and is of interest in a range of other fields, including pipelines.

One major issue that has not been properly addressed, and must be, before AE monitoring can be applied on a large scale, is that aircraft manufacturers are moving away from using wired systems. The main motivation for this is the potential for weight reduction and reduction in installation time. Removal of issues relating to wire degradation and improved accessibility are also major factors.[2] Given that an A380 has over 300 miles of cables,[5] the potential weight savings are significant. Given this move away from wired systems, it is very unlikely that anyone would want to add significant weight to the structure if the benefits achieved by doing so were not significant and beneficial in the short term. Wireless systems have other advantages, including easier integration to new or existing airframes and simpler fault detection. It has been estimated that the adoption of wireless systems could lead to cost savings over the life of an aircraft of between 14 and 60 million dollars.[2]

This means that any new SHM technology applied to an aircraft will need to be wireless, both in terms of data communication and power. For this to be effectively applied, communication would currently be via radio frequency (RF), which although can be low power is still typically the largest consumer in a wireless system.[6] One option to power a wireless system is through batteries, and although it is possible for a low-power system to operate for a long time on a battery, there are major problems in using them regarding performance at low temperature[7] and safety on board aircraft.[8] They also have only a finite life so will always need to be changed at some point. Ideally, a system would be self-sufficient and powered through energy harvesting methods, such as thermal gradients and vibration. Exact figures on the power that is available for a sensor on an aircraft from energy harvesting are difficult to estimate as it depends very much on operating conditions. Literature suggests that power harvested from vibration would be in the order of mW[9] and from thermal gradients in the hundreds of mW[10] (although only available during take-off and landing). A combination of both of these methods could power a system if it were very low power.

Manufacturers of AE hardware have developed wireless systems for commercial sale.[11–14] The devices typically require between 0.5 and 5 W to operate, depending on configuration, which although being low power is higher than that available on an aircraft through energy harvesting. These devices are all designed for application on infrastructure such as pipelines, pressure vessels or bridges where batteries can easily be replaced incrementally, or solar power is available. Their wide range of uses means that they are developed as versatile systems, where being low power is not the main requirement. Gao et al.[2] present an overview of research into wireless SHM systems. The majority of prototypes are not aimed at AE monitoring, instead at strain or vibration, meaning the sample rates are too low. Additionally, of the prototypes where power is stated none are below 100 mW, making continual operation powered by energy harvesting infeasible.

2 | OVERVIEW OF AE

AE occurs in a structure due to the sudden release of energy, for example, crack growth. From this, a high-frequency elastic wave is produced. These waves can be detected by piezoelectric sensors bonded to the surface of a structure. Monitoring this data over time gives an indication of the health of the structure, additionally locating the source of the event allowing potential areas of damage to be identified. Classification of sources can also make a distinction between events due to noise and damage.[15]

When an AE wave propagates within a plate like structure, such as an aircraft wing or pressure vessel, it travels as a Lamb wave.[3] These exist in two primary forms: symmetric and antisymmetric (or asymmetric) modes whose velocity is partially based on frequency, meaning they are dispersive. Many modes can exist; however, for this work only the principle S_0 and A_0 modes are considered. When AE is generated in a structure, a broadband wave is produced, the S_0 mode typically being a higher frequency[16] and travelling significantly quicker than the A_0 mode. Studies have also shown that in composite structures, the S_0 mode is heavily dependent on fibre orientation, travelling faster in the direction of the fibre.[17]

Knowledge that damage is occurring in a structure can be useful; however, in the case of an aircraft, it is also important to know where it is occurring. This is traditionally done using a method of Time Of Arrival (TOA) triangulation,[18] where sensors are spaced apart over the structure. This technique works well in flat, plate-like structures such as pressure vessels; however, complexity complicates matters and researchers have investigated improved techniques. Paget et al.[17] developed a method that accounted for the S_0 mode's tendency to travel at a greater velocity in certain directions in composites. Baxter et al[19] developed a mapping technique to teach the structure what TOA differences to expect for each location which has been further improved on by a number of other authors.[20–22]

Other researchers have trialled techniques where three or more sensors are bonded closely together in a tight array, as opposed to being spaced over the structure. By comparing the difference in arrival times at the sensors, there are multiple ways to predict the angle of arrival of a source. The distance a source has travelled can then be approximated by finding the difference in S_0 and A_0 arrival times and their known velocities. Figure 1 shows a waveform with clear separation of the modes. This method is called single sensor modal analysis (SSMA). An early application of this technique was developed by Sachse and Sancar[23] who used a method of manual SSMA. Aljets et al.[24,25] used a Continuous Wavelet Transform (CWT) which represents a wave's frequency relative to time, making it possible to see when certain frequencies appear within a waveform. Given that the S_0 and A_0 modes typically travel at different peak frequencies, a CWT makes it possible to identify when these frequencies are first present, and so this mode's arrival.[26,27] Although crossover of frequency does exist, the S_0 tends to travel primarily at higher values (>150 kHz).

The use of CWT for mode determination has been tested and used in both aluminium and composite structures, with both artificial Hsu-Neilson (H-N) sources (the ASTM standard for sensor calibration[28]) and real damage located.[25,26] No testing conducted on complex structures has been reported; however, it would be expected that accuracy would fall significantly if applied due to wave propagation being affected. Any thickness changes will also affect the velocity of the wave,[29] and mode conversion is known to take place, where part of the S_0 mode will change to A_0 or vice versa.[30] Any holes or edges will not only affect wave paths but cause scattering and mode conversion.[31] In aircraft structures stiffeners are very common, which will heavily attenuate a waveform.[32]

3 | WIRELESS AE

For AE to be monitored wirelessly, two hardware setup options are available. Firstly, a one sensor one Node option where each Node collects data and sends it to a central hub which performs localisation based on the data from multiple Node's. This has been applied commercially[13,14] within a wireless system; however, a limiting factor for this approach being low power is the requirement for accurate time synchronisation between Nodes. As the wave front can travel over 7,000 m/s, synchronisation needs to be in the order of μs with any error leading to high inaccuracies in localisation. This can be achieved through RF[33] or GPS[34] and must be performed very regularly due to clock drift. The aircraft industry aims to have a time synchronisation accuracy of 20 μs over a large SHM network;[2] this is too low for accurate TOA localisation. Giannì et al.[34] created a low-power single sensor Node with GPS time synchronisation, which monitored AE to locate impact on aerospace components. The system maintains a sleep mode, which at 80 mW is high, due to GPS requires locking to the timing signals. Once an event is detected the Node "wakes up," completing

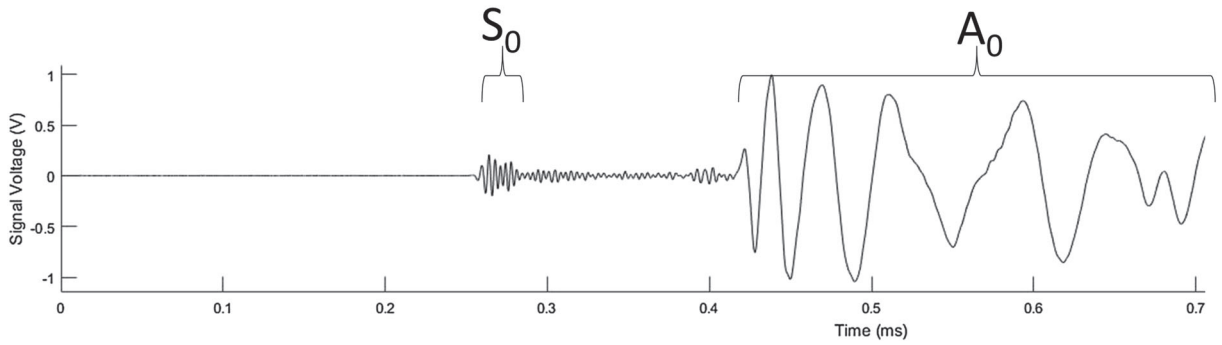

FIGURE 1 Modes within an acoustic emission signal from a composite panel. The panel (composite panel B) is described in the test method section. The H-N source 300 mm at 0° orientation from a Nano-30 sensor, amplified with Mistras 2/4/6/preamp at 40 dB gain and collected using a Mistras express 8 AE system

the time synchronisation and the rest of the processes, consuming around 360 mW. This example shows that even in a case such as impact monitoring, where operation is only occasional, a low-power single sensor Node is difficult.

The second option is to have multiple sensors connected to a single Node, with each Node operating independently of the others. This approach has been applied commercially by Mistras.[11,12] The key advantage of this is that accurate time synchronisation is not required; however, if the standard TOA approach is used, additional wiring is still required to connect the Node's to a central hub. The use of sensors bonded closely together as was done by Aljets[25] has the potential to be very effective in a wireless system as sensors, Node and energy harvesting can be all positioned together, possibly within a single housing.

4 | APPROACH OVERVIEW

4.1 | Localisation approach

For the approach taken by Aljets et al.[25] to be applicable in a wireless system, it requires some modifications to be made. In the work a CWT was used to separate the S_0 and A_0 modes; this is unsuitable for a wireless system due to power constraints. Instead, within this work, frequency filters have been used to isolate a frequency component of the S_0 and A_0 modes from the wave. The broadband nature of the modes means that a filter will not isolate the entire mode, but instead a frequency component of it, with a known velocity. From these filtered waveforms, the arrival time of each mode can be determined through a threshold crossing method. The distance of wave propagation can then be approximated through SSMA using a known dispersion value calculated using Equation 1.

$$\text{Dispersion} = \frac{1}{\frac{1}{v_{A_0}} - \frac{1}{v_{S_0}}} \tag{1}$$

To determine the angle of arrival, Aljets[25] used a method based on comparing the smallest difference in A_0 arrival time between two sensors and comparing this value to the theoretical largest possible difference in arrival time. Through Pythagoras, the angle of arrival can then be found. Preliminary testing with this technique showed that it was very susceptible to late arrival times drastically affecting the results, sometimes causing an arrival time greater than theoretical possible if a waves' arrival time was being detected accurately. This problem was mitigated a method which compares the difference in arrival between the first and second (dT_{12}) and the second and third hit sensors (dT_{23}), which is a simplification of the triangulation work presented by Kadri et al.[35] In addition to being less susceptible to late arrival predictions, the approach is tolerant to environmental and process variations, leading to a consistent repeatable result. The simplified ratio metric implementation also requires no calibration, as the wave velocities are not needed, allowing for quicker implementation.

The relationship between the ratio in wave arrival and the angle of arrival can be derived based on the vectors in.

Figure 2 as shown in Equations 2–5, which predict an angle between 0° and 60°. Software within the sensor node determines the angle of arrival by taking the first hit sensor's angle from the centre (i.e. 0°, 120° or 240°) ± the predicted angle depending on the second hit sensor. To minimise the sensor node power consumption, the angle computations are precalculated to a resolution of 1° and applied via a simple software look up table within the sensor node.

$$\frac{dT_{12}}{dT_{23}} = \frac{\sin(60-\theta)}{\sin\theta} \tag{2}$$

$$\frac{dT_{12}}{dT_{23}} = \frac{\sin 60\cos\theta - \cos 60\sin\theta}{\sin\theta} \tag{3}$$

$$\frac{d_{T12}}{dT_{23}} = \sin 60\cot\theta - \cos 60 \tag{4}$$

$$\theta = \cot^{-1}\left\{\frac{1}{\sin 60}\left(\frac{dT_{12}}{dT_{23}} + \cos 60\right)\right\} \tag{5}$$

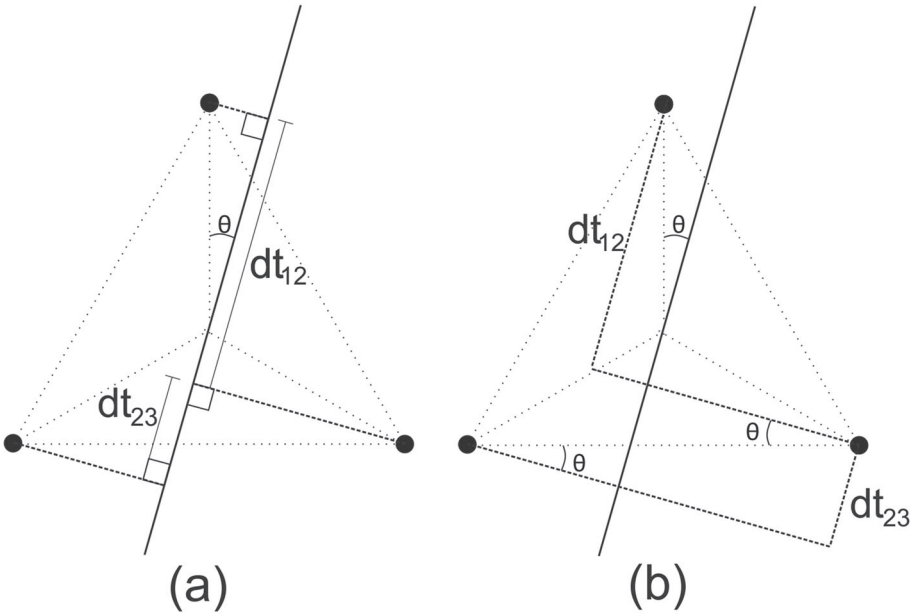

FIGURE 2 dT12/dT23 shown in terms of vectors where sensors are shown as solid circles, wave paths as solid lines and dashed lines indicating additional geometry

Within Aljets,[25] work distance was calculated at each sensor using SSMA and averaged, giving the distance from the centre of the array. Within this work, the calculation is only done at one sensor to reduce the required number of filters and hence power consumption and complexity. This leads to an error in localisation, as the angle of arrival is calculated from the centre of the array as shown in Figure 3.

The actual distance from the centre (D_a) can be found using the angle of arrival (θ) and predicted distance to the source (D_p) using trigonometry as shown in Equations 6 to 8.

$$D_s = D \times \left(\tan\tfrac{\pi}{3} - \tan\tfrac{\pi}{6}\right)/2 \tag{6}$$

FIGURE 3 Demonstration of the distance prediction problem

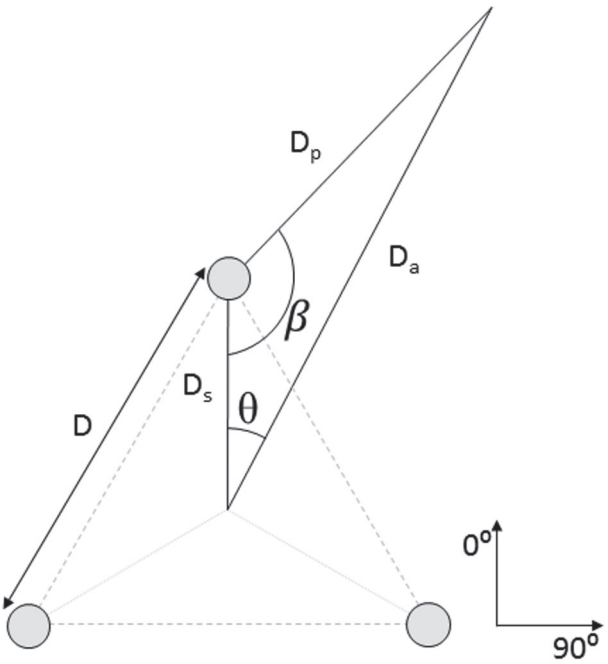

$$\beta = \pi - \theta - \sin^{-1}\left(\frac{D_s \times \sin\,\theta}{D_p}\right) \tag{7}$$

$$D_a = \sqrt{{D_s}^2 + {D_p}^2 \times 2D_s D_p\,\cos\,\beta} \tag{8}$$

4.2 | Parameter extraction

Parameter extraction is the process of taking basic parameters from a waveform. Parameters that can be extracted include amplitude, rise time, duration, counts and absolute energy; these are shown in Figure 4. Parameters are vital in order to understand the severity of an AE event, if only based on the amplitude of the signal. Studies have shown that it is also possible to distinguish between different types of damage using extracted parameters.[36] This is best performed on the Node, as transmitting an entire waveform wirelessly has a significantly greater power requirement. The importance of parameter extraction meant that each version of hardware contained an analogue to digital converter (ADC) in order to allow the extraction to be performed on the unfiltered signal from one channel. The parameters extracted were rise time, maximum amplitude, count and mean square. The mean squared is proportional to the root mean squared (RMS), other than it not having been square rooted; this was to reduce the power requirements of the sensor Node.

4.3 | Wireless data transfer

Low-power wireless communication is vital for a low-power wireless system. In a typical sensor AE data not only need to be transferred from Node to hub but messages are also sent from hub to Node. These messages could be altering settings, turning the sensor into sleep mode whilst the aircraft is grounded to save power or time synchronisation. A key advantage of using three closely spaced sensors is that time synchronisation between Nodes is not needed, as each Node operates independent of the others.

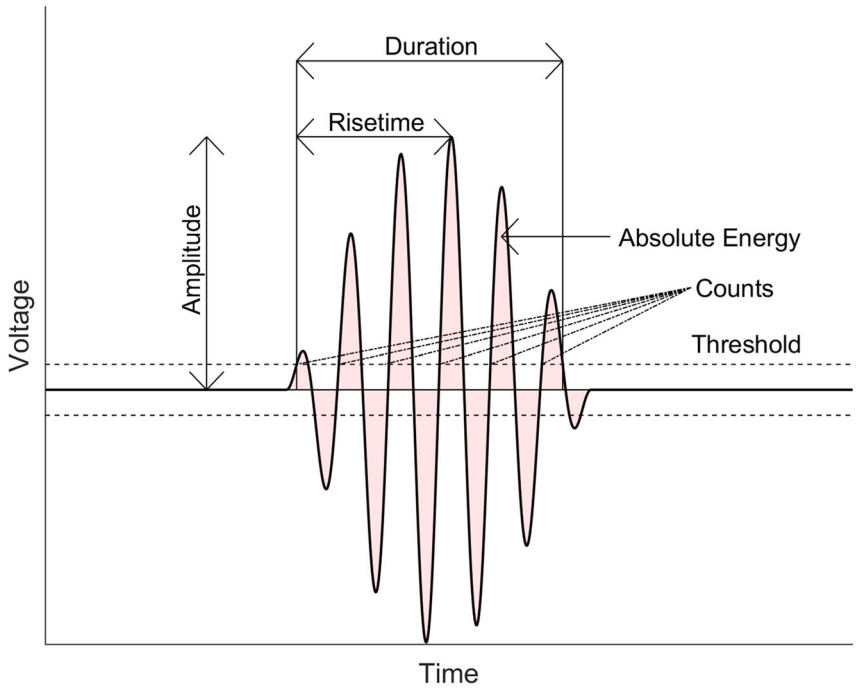

FIGURE 4 Parameters from an acoustic emission waveform

Wireless communication for this project was performed using a Nordic nRF51-series SoC device. This is an ARM Cortex M0 CPU core with an on-chip 2.4Ghz IEEE 802.15.4 compliant radio peripheral. IEEE 802.15.4 is the basis for a number of low-power, short range protocols (e.g. BLE, Gazelle, ZigBee and Thread) but is used in this application to implement a custom protocol stack that allows even lower power usage. The final module can be seen in Figure 5(a), where it is plugged into the hardware. The module allows the Node to communicate with a wireless hub (Figure 5(b)), which uses the same RF module with additional hardware and firmware.

The hub can receive messages from multiple Nodes and upload the data wirelessly via GPRS to a cloud-based network. If GPRS is unavailable, the hub can store data which can then be uploaded when possible. Figure 6 shows the flow of data from the Node to the hub and then on to the cloud. Messages can also be sent in the opposite direction; targeting a particular Node as required. This allows changes to be made to a Node wherever it is in the world, provided it is in range of a hub.

The desired reliability of data transfer must be considered when designing wireless communication protocols. In an ideal world, all data would be successfully transmitted all the time; in practice, this would be power intensive and slow, compared to risking certain messages not sending successfully. A message being sent from a hub to a Node must be received, it could be telling the Node to turn on and acquire data. On the other hand, a single event from a fatigue source that will generate thousands of events is less vital. Data are lost if either multiple Nodes send data simultaneously or the hub is sending data at the same time as a Node does. Data can also be lost in the harsh aircraft environment, which has shown to increase interference and packet loss rate.[2] To reduce the likelihood of collisions like these occurring, so called "jitter" is applied at the Node to outgoing messages. Jitter involves applying a random delay after an event and before data transmission to minimise the possibility of messages colliding when multiple Nodes detect the same event. This protocol setup is only applied in its current form when each hit is sent individually from the Node to the hub, which is useful for small scale testing where it was viewed that the loss of a single event was not a major problem. If this system were to be implemented for flight testing, it was envisaged that data would not be sent individually but clustered and only important data sent. This would reduce the traffic on the wireless network and so the power requirements of the Nodes and would require modifications to the protocols to ensure data transmission was assured.

In order to minimise the power requirements for RF communication, the Node turns on its transmitter only when required to broadcast and turns its receiver on only for a tiny "listen window" after broadcasts. A periodic "presence" broadcast is timed using an inaccurate low-power clock. This means that the hub cannot anticipate the listen window. However, the broadcast announces that the Node is listening, so when the hub receives that broadcast, it knows that that Node will hear anything it sends back provided the hub responds quickly, which it does. This process ensures reliable data transfer with only a minor increase in power consumption in each Node.

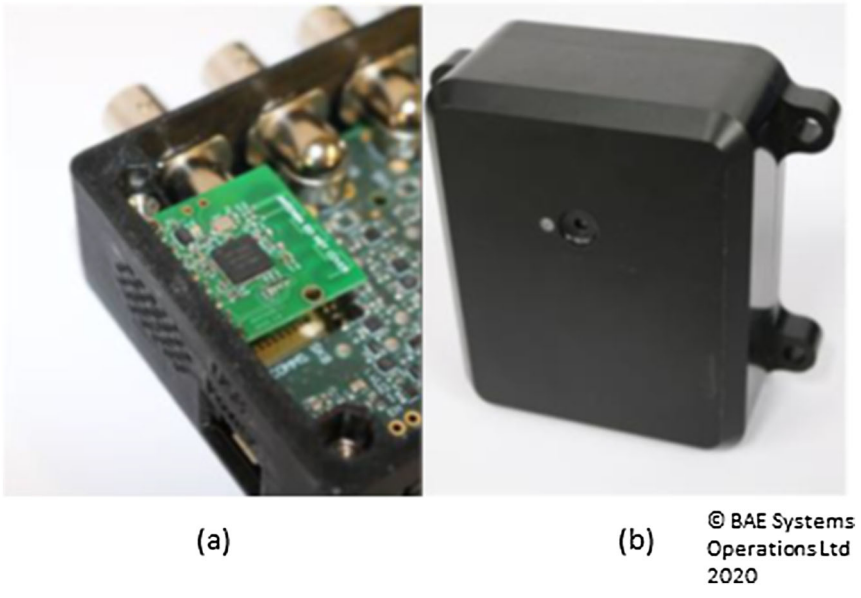

FIGURE 5 Image of wireless communication module in node (a) and wireless hub (b)

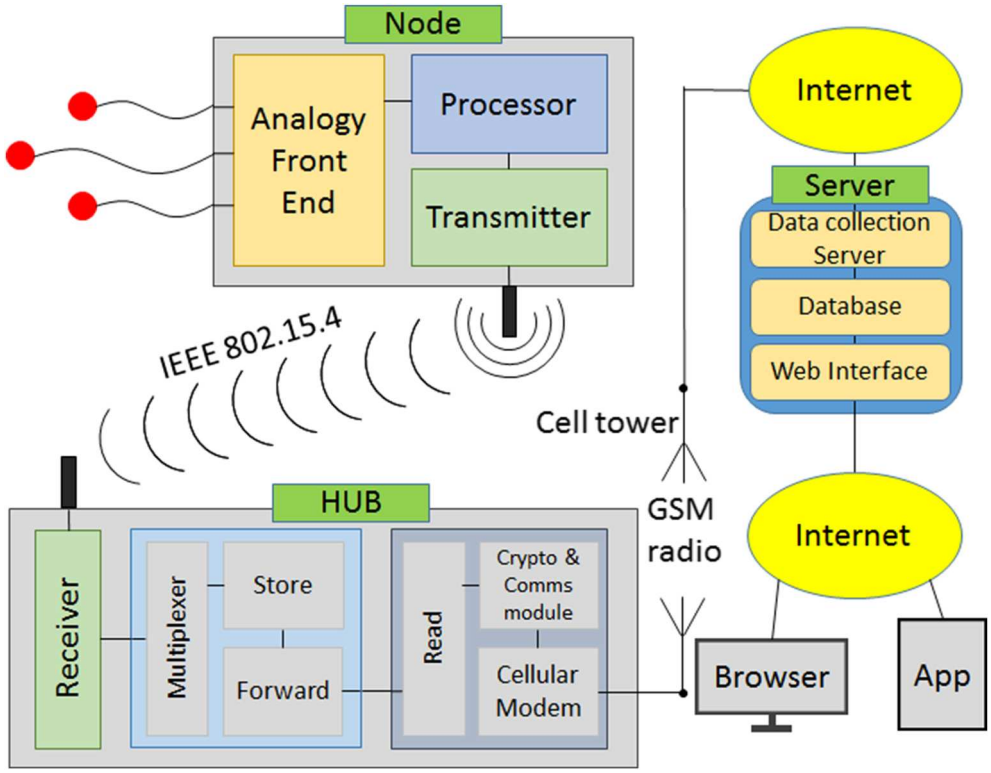

FIGURE 6 Diagram of communication from node to hub then to the server

5 | TEST METHOD

In order to test the wireless systems, three plate-like structures were used, an aluminium panel, a 0/90 composite plate (composite panel A) and a quasi-isotropic composite plate (composite panel B). Three Physical Acoustics Nano-30 sensors were bonded 75 mm apart in a triangular array on each panel, the location of which varied for each panel and is described below. A 75 mm spacing was decided on after a range of values were trialled on the aluminium panel. It was seen that bonding the sensors closer than this increased the likelihood that an identical wave was seen by all sensors, as attenuation which occurs between the sensors sometimes caused enough of a drop in amplitude for a channel to have a late arrival time. However, it also causes the time of arrival difference between the sensors to be significantly decreased, meaning any late arrivals would lead to a high level of inaccuracy in the angle prediction. A 75 mm appeared to be a suitable compromise; however, this is not optimised. Nano-30s were selected due to their small size, meaning that a more precise time of arrival prediction can be made. These are however resonant between 125 and 750 kHz, meaning they are not ideal for detecting lower frequencies; however, this was not noticed as a problem in preliminary testing.

Tests were then performed on each panel to find the characteristics of wave propagation. A H-N source was created at 100 mm from one of the sensors; a Fast Fourier Transform (FFT) was used to identify the dominant S_0 and A_0 frequencies of the propagating wave. An attenuation test was then performed at 100 mm intervals from the sensor; on the composite plates this was performed at 0°, 45° and 90°. The received waveform's peak amplitude was extracted. In all cases this was the A_0 mode. The waveforms were then passed through a 250th order 100 kHz high pass infinite impulse response (IIR) high pass filter which was deemed to fully remove the low-frequency component of the A_0 mode. The peak amplitude of the filter's output was then taken as the S_0 amplitude at this point. From this data, the rate of attenuation for the S_0 and A_0 mode was found as well as the initial S_0 amplitude of the source, which unlike the A_0 mode was not 100 dB. Finally, the S_0 and A_0 wave velocities were found using another sensor bonded with grease 150 mm from the first; a H-N source was created behind this. The difference in arrival times allows the S_0 velocity to be calculated. Passing the waveforms through an IIR band pass filter (BPF) 20 kHz above and below, the dominant A_0 frequency allowed the A_0 velocity to be found through the output's arrival time. In the composite panels, this was done at 10° increments with the outputs averaged. The 0/90 composite panel B varied by 10% and the quasi-isotropic composite panel B varied by 5%. The rate of dispersion for each panel was then found using Equation 1.

A summary of the evaluated wave parameters is shown in Table 1.

Testing was conducted on each of the structures by conducting 5 H-N sources every 100 mm over the top surface of the plate. Data were collected and analysed using the wireless system. In a small number of cases, the wireless communication did not successfully transmit the event; this was to be expected due to the low-power nature of the communication making a 100% transmission rate unachievable. In these cases another event was produced at the same location as the purpose of the testing was to assess the location accuracy, not the wireless communication.

The aluminium plate was 1,250 mm × 1,250 mm, 3 mm thick and made of 6082-T6 aluminium. The three sensors were bonded in the centre of the panel. A 25 mm space was left between the outermost test locations and the edge of the panel. Once data had been collected from the simple plate, complexity was added. To do this, four extruded 6082-T6 aluminium "C"-shaped stiffeners were attached at regular intervals to the plate with an identical plate bonded to the bottom. Two of the stiffeners were bonded using Araldite 420 A/B and the other two using twenty-five 4 mm aluminium rivets attached every 5 mm in a zig-zag fashion. The sensors were left bonded whilst this change was made, allowing a test as identical to the original as possible to be performed. The test area, complexity and sensor locations are shown in Figure 7.

Composite panel A was made using eight plies of HelPly® M21 unidirectional pre-preg, with a $(0/90)_{2s}$ layup. The created panel is 1 m × 1 m and 2 mm thick. The 0/90 layup means that the plate is anisotropic, causing wave S_0 mode velocity to be dependent on direction. Preliminary testing using a wired system indicated that the range of the technique was larger than the maximum distance of 0.7 m that bonding the sensors in the centre of the panel would allow

TABLE 1 Test specimen wave parameter summary

	Propagation frequency (kHz)				Attenuation rate (dB/m)		
Specimen	**S_0**	**A_0**	**Average dispersion (m/s)**	**Direction**	**A_0**	**S_0**	**S_0 amplitude (dB)**
Aluminium panel	240	70	6,300	N/A	23	44	80
Composite panel A	300	60	2,200	0	34	8	62
				45	35	43	
				90	32	18	
Composite panel B	300	50	2,100	0	30	33	82
				45	28	43	
				90	18	36	

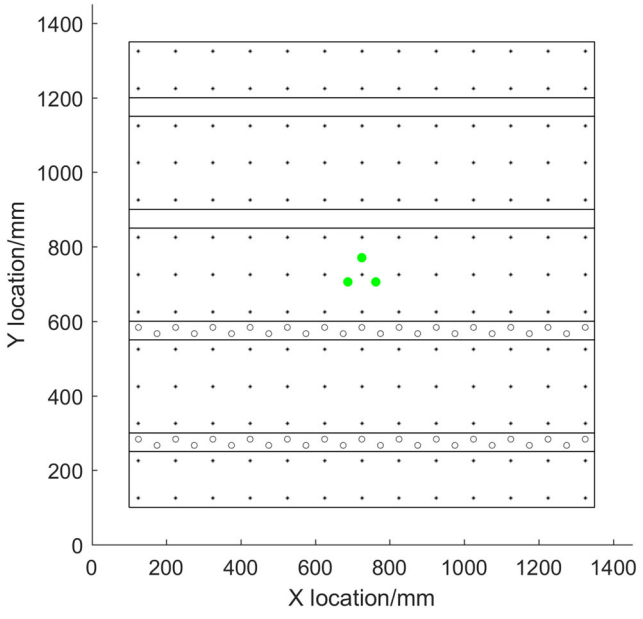

FIGURE 7 Location of sensors and complexity on aluminium panel. Sensors shown as filled circles and rivets as non-filled circles. Test locations shown as crosses

to be tested. Hence, they were bonded with a centre of $x = 0.29$ m and $y = 0.3$ m. A schematic of the plate with the sensor and test locations is shown in Figure 8. No additional modifications were made to the plate after its construction.

Composite panel B was manufactured using 16 plies of UT210 38% RWB unidirectional carbon fibre pre-preg with a lay-up of $(0/45/90/-45)_{2S}$, creating a quasi-isotropic panel. The panel was vacuum bagged and a porous membrane used to remove excess resin whilst being cured within an autoclave. The panel was C-scanned to ensure no significant defects were present. The final dimensions of the panel were 900 mm × 900 mm and a thickness of 3.5 mm. As with the previous panel, the sensors were not positioned in the centre, instead they were bonded at $x = 0.3$ m $y = 0.2$ m from the bottom left corner of the panel which allowed for a maximum distance of 0.92 m. The outermost test locations were 50 mm from the edge of the panel.

Once testing had been completed on the simple panel, carbon fibre "L"-shaped stiffeners (25 mm × 25 mm and 3 mm thick made from twill weave) were bonded to the surface of the panel 200 mm apart using Araldite 420 a/b. These were added one at a time and testing conducted in-between the bonding of each. As with the aluminium structure, the sensors were left in place for every test. The location of the test points, complexity, sensor locations and the order in which the stiffeners were bonded is shown in Figure 9.

6 | HARDWARE DEVELOPMENT

The sensor node hardware and software were designed to detect AE events, find their angle of arrival and predict their travelled distance; the node was manufactured by BAE Systems Rochester. Prior to finalising the sensor node design, multiple waveforms were captured with oscilloscopes across various composite and aluminium structures using the three sensor approach, by both the BAE Systems and Cardiff University teams. This enabled a wide range of test data to be built up, which were used to directly drive the analogue front end of the computer simulations of the hardware; hence, the design was optimised prior to a final design build being committed to. The key challenges were the lowest operating power, the smallest physical size and the optimum performance.

An additional fourth channel was added to the design for a future expansion option. An image of the final hardware developed is shown in Figure 10, with the RF Node shown on the left-hand side as a small plug in mezzanine. The large BNC connectors shown enable easy test connection; micro connectors in a final build replace these.

6.1 | Overview

Previous implementation of the three closely spaced sensor location techniques has always been conducted using commercial wired systems which were able to acquire waveforms. These waveforms were post processed using digital

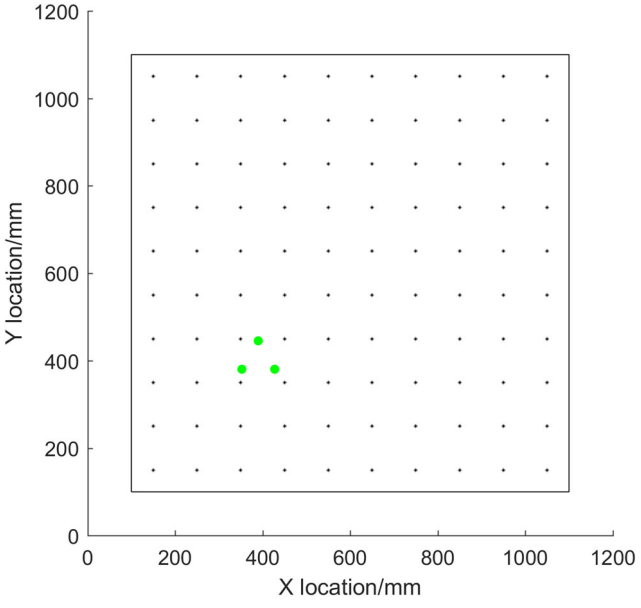

FIGURE 8 Location of sensors on composite panel a. Sensors shown as filled circles and test locations as crosses

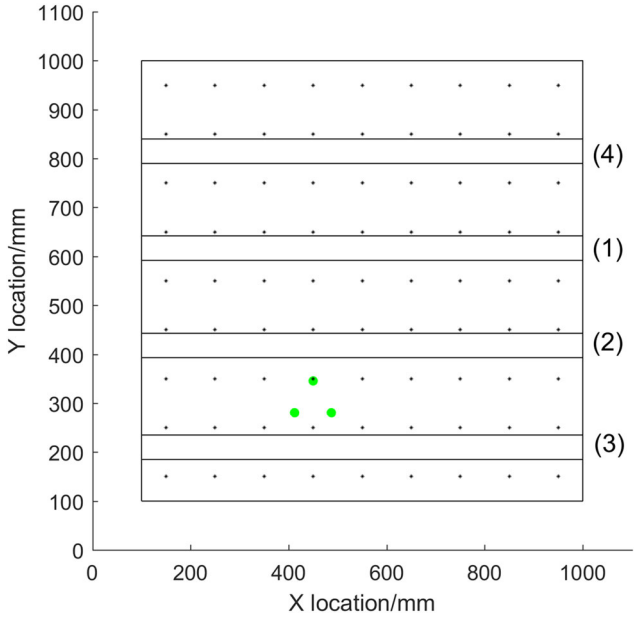

FIGURE 9 Location of sensors and complexity on composite panel B. Sensors shown as filled circles and test locations as crosses. Labels show order of stiffener bonding

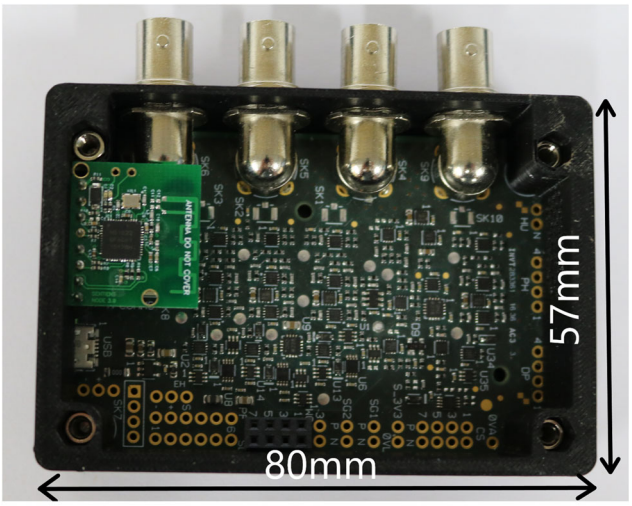

FIGURE 10 Hardware with wireless communication board within 3D printed case

frequency filters or a CWT in order to perform SSMA on the waveforms to determine the arrival times of the S_0 and A_0 modes and so the location of the source. In the case of a wireless system, converting waveforms into digital form using an ADC is possible; however, frequency analysis on-board, however, is not feasible due to power and time requirements. The remaining option is to send entire waveforms wirelessly to be processed elsewhere, but this again would consume too much power.

Given the low-power levels available from the energy harvesting, the approach taken within the Node design was to process the events within the Node and therefore to minimise the data transmissions required. With each Node acting autonomously, the tight time synchronisation between the Nodes was removed and the power requirements further reduced.

To reduce the power requirements, analogue rather than digital filters or a CWT was used, with their cutoff frequencies set to detect either the S_0 or A_0 mode. Their cutoff frequencies were based on FFT results from the aluminium panel and composite panel A (at the time of manufacture, composite panel B had not been made). The A_0 mode was detected using a BPF around 100 kHz (approximately 60 to 140 kHz). The S_0 mode from an AE event is the first that arrives at the sensors, so a narrow filter is not needed to detect its arrival; however, it does reduce the possibility of the system triggering from noise. A BPF around 150–300 kHz was therefore used to isolate the S_0 mode.

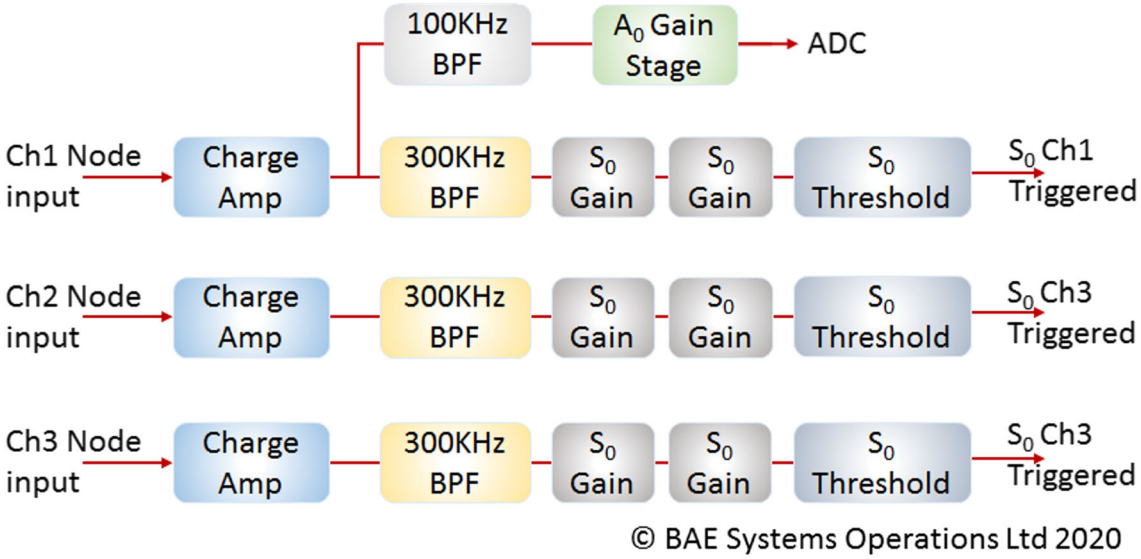

FIGURE 11 Analogue front-end architecture for node

Figure 11 provides a top-level overview of the input conditioning circuitry for the Node; the gain and threshold levels were controllable via software whilst the filter characteristics were pre-set. The filtered channel data and levels were digitalised by the on-Node processor to determine the event parameters. Given Lamb wave may cross the sensor array in under 10 μs, the implementation of the arrival time prediction needed to be sub microsecond for accurate angle prediction.

The BAE Systems team designed the event detection system to operate with the whole sensor node in deep sleep mode, then wake up on the arrival of the first A_0 signal in the array, digitise the A_0 event waveform and to measure the time of arrivals difference between the three sensors. The successful design implementation achieves all this whilst measuring the time of arrivals to a resolution of < 50nS.

As previously stated, an additional fourth channel was also added to provide more flexibility on the application of the Node. The fourth channel facilitated a more traditional TOA triangulation over the four sensors and an application for impact detection. Additional on-board accelerometers and environmental sensors such as temperature, pressure and humidity were also added together with on board Real Time Clock, NVM (Flash and FRAM) and a Micro SD card interface. Additional external Interfaces for external strain gauges, corrosion sensors and additional accelerometers were also provided. These capabilities were added to broaden the future application of the Node and are not covered within this paper.

6.2 | Testing

To analyse the dynamic power usage of the Node, the team used the power measurement facility of the Silicon labs ARM development system, in this case a Silicon Labs "EFM32 Wonder Gecko" development board was used. This development board has a 3.3 V output, which is able to power our wireless Node, whilst placing its own processor in a low-power mode requiring 6 μW to run the board, a negligible amount. The Simplicity Studio energy profiler (software by Silicon Labs) was then used to analyse the Node's power requirements, which will be the Node's power consumption plus the negligible power the development board requires. This allowed the Node's dynamic power to be recorded and evaluated at a rate of 5,000 Hz for each stage of operation.

For the processes which are performed over extended periods of time, the average power was found; these were sleep mode and when waiting for an event to be detected. For shorter processed, the time period and so total energy were also found. These were when the RF was listening for an incoming message, when an event was being processed and when the RF module was preparing and sending a message. These values are shown in Table 2.

TABLE 2 Power consumption of node in a variety of functions/performing certain tasks

	Sleep	Event monitoring	RF listen window	Event processing	RF transmission
Time (ms)	-	-	103	5	176
Average power (mW)	0.33	17.44	43.4	10.0	39.5
Total energy (mJ)	-	-	4.47	0.05	6.95

Abbreviation: RF, radio frequency.

Location testing was conducted on the three simple plates. The maps of the absolute errors for each are shown in Figure 12(a), 12(c) and 12(d). For the Aluminium panel, complexity was then added and another test performed, the error map for which is shown in Figure 12(b). Composite panel B then had complexity added one stiffener at a time and a test performed after each. After the addition of the third stiffener, no data could be accurately located beyond the location where the fourth stiffener was to be bonded, meaning accuracy was not affected with the addition of the fourth stiffener. A map of the errors for the complex composite panel B is shown in Figure 12(e).

A summary of the average error, angle error and distance prediction error is shown in Table 3 or each of the tests. In some cases, no approximation could be made for a location; in these cases, the average error was set to 300 mm so a comparison could be made between testing. Table 3 also shows the percentage of data for each test that is within a certain level of accuracy, within 50 mm an event is said to have been very well located, within 100 mm it has been located adequately and within 200 mm it has been located.

7 | MODIFIED HARDWARE

The testing conducted using the Node showed good accuracy in simple plates but poor performance when complexity was added. This was primarily due to S_0 to A_0 mode conversion causing low-frequency wave to arrive prior to the bulk A_0 mode combined with a heavily attenuated A_0 mode, making its arrival time very difficult to detect. This led to very high inaccuracy in both the angle and distance prediction, which rely on the modes' arrival times being precise.

Testing with a wired system showed that better accuracy could be achieved in complex structures if the S_0 mode was used to predict the angle of arrival. This has an important limitation, as the S_0 mode is significantly more affected by fibre orientation than the A_0. This means non-quasi-isotropic structures, such as the 0/90 composite panel A, will have high errors. Using the S_0 mode to predict the angle does not eliminate the need for an A_0 arrival time, as the distance prediction relies on it. Instead, for this work the A_0 mode's peak amplitude was used as an approximation of its arrival time. It was assumed that the peak arrival time would always be part of the A_0 mode, which prior testing had indicated. It is also based on the assumption that this point would typically be at a constant frequency meaning it would travel at a relatively constant dispersion to the S_0 mode. To do this required recalculation of wave dispersion rate.

7.1 | Overview

To implement the proposed technique, changes necessitated a large change to the hardware analogue front end of the Node, effectively changing over the 100 kHz BPF and 300 kHz HPF filter stages and increasing the associated gain stages whilst still maintaining the lowest power budget. However, the increased gain requirements on the 300 kHz filter channels did result in an increased power requirement for the Node.

An overview of the architecture is shown in Figure 13. The original Node's A_0 gain stages and filters were exchanged for similar ones to those used for the original S_0 channel. This was done in reverse for the original S_0 mode, changing it to an A_0 filter and gain stage.

The Node's processor uses the arrival of the first S_0 event to time the difference in arrival times for the other two S_0 channels and the arrival of the selected A_0 channel.

The event's angle of arrival can then be calculated from these three values. The parameter extraction algorithm extracts the rise time from the digitalised 100 kHz BPF waveform from channel 1 which gives an approximation of distance.

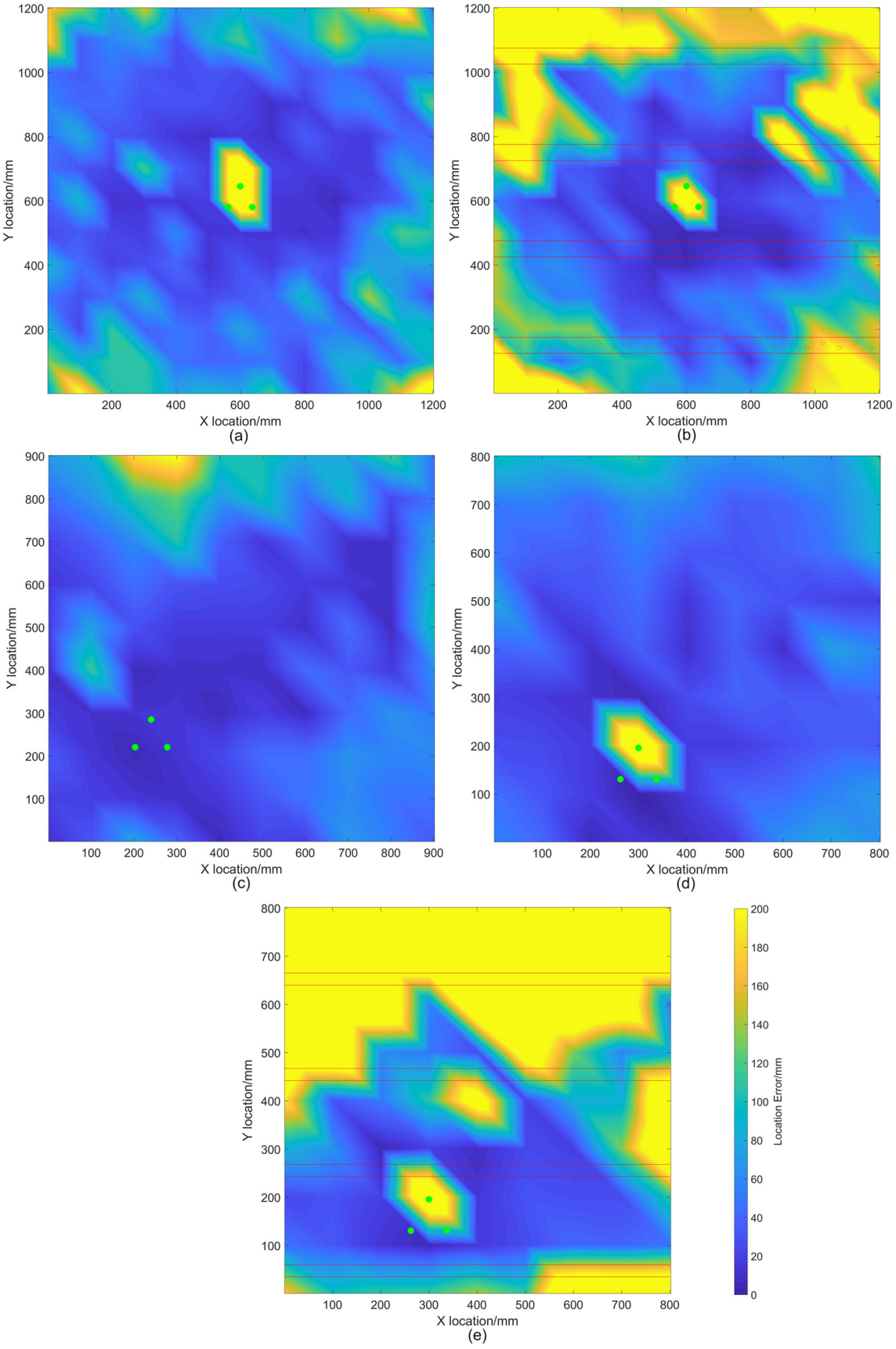

FIGURE 12 Absolute location error map for simple aluminium panel (a), complex aluminium panel (b), composite panel A (c), simple composite panel B (d) and composite panel B with four stiffeners (e). All errors capped at 200 mm

TABLE 3 Error and accuracy data from testing where the number of stiffeners bonded to composite B are specified

		Aluminium			Composite B				
		Simple	Complex	Composite A	0	1	2	3	4
Angle error (°)		3.8	7.1	3.1	3.5	7.3	14.0	16.8	16.8
Distance error (mm)		26.4	44.1	18.2	21.9	52.2	122.0	131.1	131.1
Total error (mm)		62.0	107.3	44.5	45.5	78.6	142.0	161.8	161.8
Data within given distance (%)	50 mm	62	40	69	70	58	48	36	36
	100 mm	83	60	90	93	81	58	45	45
	200 mm	93	80	99	99	86	60	55	55

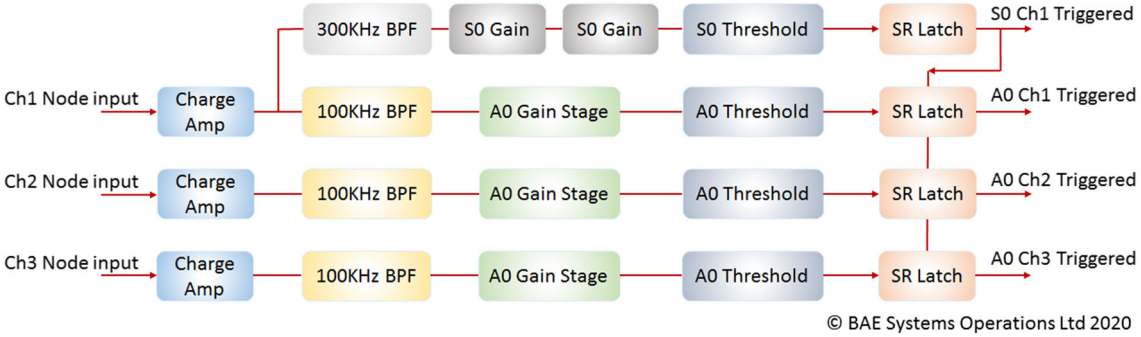

FIGURE 13 Analogue front-end architecture for modified node

7.2 | Testing

As with the previous version of the hardware, the modified Node's power consumption was evaluated during a range of operation modes. The results from this showed an increase in the power required when waiting for an event from 17.44 to 22.7 mW.

Two significant problems were experienced as a result of this upgrade. Firstly, the imitations on the implementation of the increased gain stages on the existing design lead to small but varying DC offset between the channels, which varied dependant on the channels gain. This meant that threshold levels needed to be much higher than ideal, reducing the accuracy of arrival time approximation and so angle prediction accuracy. The solution required an update to the base PCB was not possible within the project timescales.

The second problem was that the A_0 gain stage was amplifying the signal too much within the aluminium panel where its attenuation was less. This caused the ADC to max out even at its lowest amplification value meaning that the modification to trigger from the rise time of the A_0 mode was not possible, as the peak could not be detected. This meant that the distance could not be approximated in the aluminium panel with this hardware. The average angle error for this testing was 4.9^0.

As anticipated, using the S_0 mode to predict the angle meant that localisation was not possible in the 0/90 anisotropic composite panel A. This was not a problem with composite panel B and a location error map for the complex panel can be seen in Figure 14. The location accuracy and average errors for the modified and original hardware for the complex panel are shown in Table 4.

8 | DISCUSSION

Within this work, the development and testing of a wireless AE system have been presented. This system is lower power than any systems currently commercially available. This was achieved by utilising the three closely spaced sensor methods, which removed the need for time synchronisation between Nodes. Testing using the system consisted of

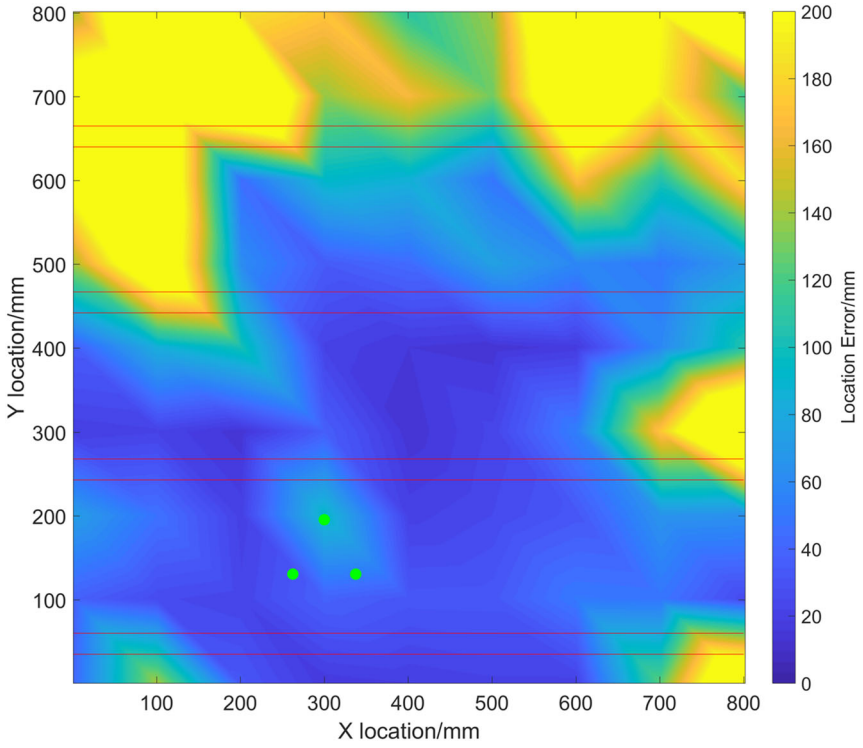

FIGURE 14 Absolute location error map for composite panel B stiffeners

		Original	Modified
Angle error (°)		16.8	4.7
Distance error (mm)		131.1	68.7
Total error (mm)		161.8	101.4
Data within given distance (%)	50 mm	36	45.9
	100 mm	45	65.2
	200 mm	55	79.3

TABLE 4 Location accuracy and errors for complex composite panel using original and modified hardware

locating H-N sources within simple and complex structures. This is limited, and further testing to locate real damage should be conducted in the future.

The location testing with the original hardware showed that it was very effective in simple structures, the only significant errors occurring at the corner/edges of the panel, which were a result of reflections from the edges of the panel. The addition of complexity to both panels significantly reduced the accuracy and range of the system. This was due to S_0 to A_0 mode conversion making the A_0 mode's arrival time difficult to predict; this was made more difficult by the A_0 mode's increased attenuation rate compared to the S_0 mode's when crossing stiffeners.[32]

This difficulty in detecting the A_0 mode led to a modification to the hardware, which enabled the angle prediction to be made from the S_0 arrival at each of the sensors. As the panels were already modified, it was not possible to trial this system on simple structures to directly compare accuracy with the unmodified system. On both complex structures, however, the angle accuracy and the operational range were significantly increased. This comes at the cost of the system being limited for anisotropic structures. The 0/90 composite is an extreme example, but it can be expected that any non-quasi-isotropic will have an error if the angle is predicted from the S_0 mode. The modifications to the A_0 mode prediction were less successful. Due to the high gain, it was not possible to predict the peak amplitude and so an arrival time. A reduction in average error was seen on the complex panel; however, it was still high and limited in terms of range. One potential improvement is better, or even bespoke per specimen, selection of A_0 filters. In the case of the complex composite panel B, which was manufactured after the hardware, the peak A_0 frequency fell outside of the BPF range.

The units designed were both very low power. As anticipated, the RF communication was the most power intensive part of the process. The need for this could be reduced significantly if data were to be clustered and only transmitted once a certain number of events were seen in one location. A software module design scheme for this was produced but was not coded into the final Node due to the type of testing that was being undertaken. A slight increase in power was seen when the hardware was modified, which was to be expected as the modification was made with the aim of improved performance with less consideration of power. It is very possible that with the correct power management, this hardware could operate long term on an aircraft structure by energy harvesting from a combination of vibration and thermal gradients.

It is clear that more testing is needed with the wireless system, primarily to detect real damage from static and fatigue testing in complex structures. This would be better achieved with a design update of the analogue front-end and re-spin of the hardware to apply what the modified hardware did. This should remove the issues with the ADC maxing out due to too high gains and the varying DC offset. Alternative methods for accurately predicting the arrival of the A_0 mode should also be investigated.

9 | CONCLUSIONS

This paper has presented an overview of a novel low-power wireless AE system capable of locating artificial AE sources using a location approach developed from the work by Aljets. This was tested in simple and complex plate like structures made from aluminium and composite. Two iterations of hardware have been shown, the second being more effective in complex structures; however, problems arose due to the retrofit. The typical complexity of an aircraft structure may limit the application and exploitation of the AE sensor to specific areas, mainly due to the A_0 and S_0 mode conversion and the limited detection range. These limitations could be improved through signal processing on-board the node. Using the three closely spaced sensor technique has allowed all sensors to be connected to a central hub, so removing the requirement for power intensive time synchronisation to avoid excess cabling. The power consumption of this hardware is very low, and it may well be feasible to power through energy harvesting methods on board an aircraft structure.

ACKNOWLEDGEMENT

This work was funded by the Innovate UK project SENTIENT, project reference 101657.

ORCID

Stephen Grigg https://orcid.org/0000-0002-5317-7139

REFERENCES

1. Mangalgiri PD, Harinarayana K. Structural Health Monitoring. In: Prasad NE, Wanhill HRJ (eds) *Aerospace Materials and Material Technology* Vol. 2. Springer, 2016:449-477.
2. Gao S, Dai X, Hang Y, Guo Y, Ji Q. Airborne Wireless Sensor Networks for Airplane Monitoring System. *Wireless Communications and Mobile Computing*. 2018;2018:1-18. https://doi.org/10.1155/2018/6025825
3. Lamb H. On waves in an elastic plate. *Proc R Soc London Ser a*. 1917;93:114-128.
4. Nair A, Cai CS. Acoustic emission monitoring of bridges: review and case studies. *Eng Struct*. 2010;32(6):1704-1714.
5. Yedavalli RK, Belapurkar RK. Application of wireless sensor networks to aircraft control and health management systems. *J Control Theory Appl*. 2011;9(1):28-33.
6. Anastasi G, Conti M, Di Francesco M, et al. Energy conservation in wireless sensor networks: a survey. *Ad Hoc Networks*. 2009;7(3):537-568.
7. RTCA SC-135. Environmental Conditions and Test Procedures for Airborne Equipment, DO-160E. RTCA; 2004.
8. Civil Aviation Authority CAA. Lithium batteries, 2015. https://www.caa.co.uk/Commercial-industry/Airports/Safety/Dangerous-goods/Lithium-batteries/
9. Wei C, Jing X. A comprehensive review on vibration energy harvesting: modelling and realization. *Renew Sustain Energy Rev*. 2017;74:1-18.
10. Samson D, Kluge M, Becker T, Schmid U. Wireless sensor node powered by aircraft specific thermoelectric energy harvesting. *Sensors Actuators A Phys*. 2011;172(1):240-244.
11. MISTRAS. 1284: the first multi channel wireless acoustic emission system. 2013.
12. MISTRAS. Micro-SHM product data sheet, 2017. https://www.physicalacoustics.com/content/literature/small_systems/Micro_SHM_Product_Data_Sheet.pdf

13. Soundwel. SAEW2 distributed acoustic emission, 2017. http://www.soundwel.cn/pro/235.html
14. Interunis. Interunis Product Catalog, 2016. http://interunis-it.ru/netcat_files/120/171/PRODUCT_CATALOG_INTERUNIS_IT_2016.pdf
15. McCrory JP, Al-Jumaili SK, Crivelli D, et al. Damage classification in carbon fibre composites using acoustic emission: a comparison of three techniques. *Compos Part B Eng*. 2015;68:424-430.
16. Surgeon M, Wevers M. Modal analysis of acoustic emission signals from CFRP laminates. *NDT & E International*. 1999;32(6):311-322. https://doi.org/10.1016/s0963-8695(98)00077-2
17. Paget CA, Atherton K, O'Brien E. Triangulation algorithm for damage location in aeronautical composite structures. In: *Proceedings of the 4th International Workshop on Structural Health Monitoring* (F. Chang, ed.), (Stanford, CA, USA); 2003:363-370.
18. Miller KR, Hill EK. Acoustic emission testing. In: *Non-Destructive Testing Handbook*. USA: American Society of Nondestructive Testing; 1987.
19. Baxter MG, Pullin R, Holford KM, Evans SL. Delta T source location for acoustic emission. *Mech Syst Signal Process*. 2007;21(3): 1512-1520.
20. Al-Jumaili SK, Pearson MR, Holford KM, et al. Acoustic emission source location in complex structures using full automatic delta T mapping technique. *Mech Syst Signal Process*. 2016;72:513-524.
21. Pearson MR, Eaton M, Featherston C, Pullin R, Holford K. Improved acoustic emission source location during fatigue and impact events in metallic and composite structures. *Struct Heal Monit*. 2017;16(4):382-399.
22. Holford KM, Eaton MJ, Hensman JJ, et al. A new methodology for automating acoustic emission detection of metallic fatigue fractures in highly demanding aerospace environments: an overview. *Prog Aerosp Sci*. 2017;90:1-11.
23. Sachse WH, Sancar S. Acoustic emission source location on plate-like structures using a small array of transducers. *J Acoust Soc Am*. 1987;81(1):206-206. https://doi.org/10.1121/1.394998
24. Aljets D, Chong A, Wilcox S. Acoustic emission source location during the monitoring of composite fracture using a closely arranged sensor array. In: Proceedings of the ASME 2011 International Design Engineering Technical Conferences & Computers and Information in Engineering Conference. 2011:1-8.
25. Aljets D, Chong A, Wilcox S, Holford K, et al. Acoustic emission source location on large plate-like structures using a local triangular sensor array. *Mech Syst Signal Process*. 2012;30:91-102.
26. Jingpin J, Bin W, Cunfu H. Acoustic emission source location methods using mode and frequency analysis. *Struct Control Heal Monit*. 2008;15(4):642-651.
27. Maji AK, Satpathi D, Kratochvil T. Acoustic emission source location using lamb wave modes. *J Eng Mech*. 1997;123(2):154-161.
28. ASTM. E650 / E650M-17, Standard Guide for Mounting Piezoelectric Acoustic Emission Sensors. ASTM International, West Conshohocken, PA; 2017, www.astm.org
29. Mook G, Pohl J, Simonin Y. Lamb Wave Generation, Propagation, and Interactions in CFRP Plates. In: Lammering R, Gabbert U, Sinapius M, et al. (eds) *Lamb-Wave Based Structural Health Monitoring in Polymer Composites*. Springer International Publishing, 2018: 443-460.
30. Cho Y. Estimation of ultrasonic guided wave mode conversion in a plate with thickness variation. *IEEE Trans Ultrason Ferroelectr Freq Control*. 2000;47:591-603.
31. Cho Y, Rose JL. A boundary element solution for a mode conversion study on the edge reflection of Lamb waves. *J Acoust Soc Am*. 1996; 99(4):2097-2109.
32. Marks R, Clarke A, Featherston C, Paget C, Pullin R. Lamb wave interaction with adhesively bonded stiffeners and disbonds using 3D vibrometry. *Appl Sci*. 2016;6(1):12-20. https://doi.org/10.3390/app6010012
33. Akhlaq M, Sheltami TR. RTSP: an accurate and energy-efficient protocol for clock synchronization in WSNs. *IEEE Trans Instrum Meas*. 2013;62(3):578-589.
34. Giannì C, Balsi M, Esposito S, et al. Low-power global navigation satellite system-enabled wireless sensor network for acoustic emission localisation in aerospace components. *Struct Control Heal Monit*. 2020:1-13.
35. Kadri U, Crivelli D, Parsons W, Colbourne B, Ryan A. Rewinding the waves: tracking underwater signals to their source. *Sci Rep*. 2017;7 (1):1-12, 13949.
36. Crivelli D, Guagliano M, Monici A. Development of an artificial neural network processing technique for the analysis of damage evolution in pultruded composites with acoustic emission. *Compos Part B Eng*. 2014;56:948-959.

How to cite this article: Grigg S, Pullin R, Pearson M, et al. Development of a low-power wireless acoustic emission sensor node for aerospace applications. *Struct Control Health Monit*. 2021;e2701. https://doi.org/10.1002/stc.2701